Bioturbation depths, rates and processes in Massachusetts Bay sediments inferred from modeling of ^{210}Pb and $^{239+240}Pu$ profiles

John Crusius*, Michael H. Bothner

U.S. Geological Survey

384 Woods Hole Road

Woods Hole, MA 02543

Christopher K. Sommerfield

University of Delaware

College of Marine Studies

Lewes, Delaware 19958

running head: modeling bioturbation in Massachusetts Bay

keywords: bioturbation, radionuclides, sediment-mixing model, non-local mixing, food-caching

*corresponding author: email address: jcrusius@usgs.gov

Abstract

Profiles of ^{210}Pb and $^{239+240}$Pu from sediment cores collected throughout Massachusetts Bay (water depths of 36-192 m) are interpreted with the aid of a numerical sediment-mixing model to infer bioturbation depths, rates and processes. The nuclide data suggest extensive bioturbation to depths of 25-35 cm. Roughly half the cores have ^{210}Pb and $^{239+240}$Pu profiles that decrease monotonically from the surface and are consistent with biodiffusive mixing. Bioturbation rates are reasonably well constrained by these profiles and vary from ~0.7 to ~40 $cm^2\,yr^{-1}$. As a result of this extensive reworking, however, sediment ages cannot be accurately determined from these radionuclides and only upper limits on sedimentation rates (of ~0.3 cm yr^{-1}) can be inferred. The other half of the radionuclide profiles are characterized by subsurface maxima in each nuclide, which cannot be reproduced by biodiffusive mixing models. A numerical model is used to demonstrate that mixing caused by organisms that feed at the sediment surface and defecate below the surface can cause the subsurface maxima, as suggested by previous work. The deep penetration depths of excess ^{210}Pb and $^{239+240}$Pu suggest either that the organisms release material over a range of >15 cm depth or that biodiffusive mixing mediated by other organisms is occurring at depth. Additional constraints from surficial sediment ^{234}Th data suggest that in this half of the cores, the vast majority of the present-day flux of recent, nuclide-bearing material to these core sites is transported over a timescale of a month or more to a depth of a few cm below the sediment surface. As a consequence of the complex mixing processes, surface sediments include material spanning a range of ages and will not accurately record recent changes in contaminant deposition.

Introduction

Bioturbation of coastal sediments by benthic organisms can have profound effects on sedimentary characteristics. Bioturbation can transport newly deposited material to depths of tens of centimeters, which has many biogeochemical consequences. Labile organic matter can thus be transported to greater depths than would otherwise occur (Jumars et al., 1990). Downward transport by bioturbation can also sequester contaminants at depths where they will not be resuspended into the water column, and where they will encounter a reducing environment, potentially impacting their mobility. Furthermore, mixing of material of varying ages by bioturbation leads to a reduction in the temporal resolution obtainable from sedimentary records. In this manner, the fate of material transported by bioturbation can be altered on timescales of days to centuries.

The radionuclides ^{210}Pb and $^{239+240}$Pu are commonly measured in sediments as tracers of both bioturbation and sedimentation. A flux of ^{210}Pb occurs to the surface of sediments as the result of the decay of radon in the atmosphere, a gaseous decay product of naturally occurring uranium. ^{210}Pb is particle-reactive and quickly sorbs to atmospheric aerosols and, once it reaches surface waters, to settling particulate matter. As a consequence of its 22.3-year half-life, ^{210}Pb provides information about particle reworking and sedimentation over timescales of roughly 100-150 years (Robbins, 1978). $^{239+240}$Pu has been distributed globally by atmospheric testing of nuclear weapons. Significant fallout commenced in 1950 and peaked in 1963. This nuclide is also found in surficial sediments because it is also particle reactive. Pu is used as a chronometer in

sediments either by assuming its peak in activity corresponds to the fallout peak in 1963 or its first detection corresponds to the onset of fallout in 1950. Where benthic organisms have been active, sedimentary Pu distributions can also be used to constrain bioturbation rates and depth (Smith et al, 1986; Anderson et al., 1988). The radionuclide ^{234}Th is derived from decay of water-column ^{238}U. Because Th is particle-reactive, ^{234}Th is rapidly delivered to the seafloor. Its short half-life (24 d) implies that presence of "excess" ^{234}Th in surficial sediment (that present in excess of the amount in secular equilibrium with the ^{238}U activity) is a useful indicator of successful core-top recovery and short-term bioturbation rates.

This study interprets profiles of ^{210}Pb and $^{239+240}$Pu from sediments of Massachusetts Bay, a coastal bay just seaward of Boston Harbor (Figure 1). Because of the severe degree of contamination of Boston Harbor, its sediments and those of Massachusetts Bay have been studied and monitored for years to evaluate the change in contaminant concentrations in response to decreases in regional contaminant sources and to local improvements in greater Boston's sewage treatment system (Bothner et al., 1998). In this paper, the radionuclides ^{210}Pb and $^{239+240}$Pu are interpreted with the aid of a numerical sediment-mixing model to infer processes, depths and rates of bioturbation and to determine whether these nuclides can constrain sedimentation rates in Massachusetts Bay.

Materials and Methods

Sediment cores were collected from the *R.V. ARGO MAINE* in May 1992 using a hydraulically damped gravity corer. This instrument is specifically designed to sample

the sediments with minimal disturbance of the sediment-water interface (Pamatmat, 1971; Bothner et al., 1997). Cores were maintained in a vertical position and kept on ice or refrigerated until they were processed. The sediment was extruded from the barrel using a vertical rack, a piston inserted at the bottom of the barrel, and a long-throw hydraulic jack. Sample thickness was either 1 or 2 cm; material in direct contact with the barrel was trimmed off and discarded. The sediment samples were dried to constant weight at 60 degrees C in a radiant oven with filtered air. The dry samples were disaggregated in an agate mortar and pestle.

^{210}Pb was determined on 10-50 grams of disaggregated sample sealed in counting jars and stored for at least 20 days to allow for the in-growth of ^{222}Ra and ^{214}Pb to approximate equilibrium values. Activities were determined by counting samples for approximately 2 days using a planar germanium detector (Canberra Industries, Inc. Model GL2020S) calibrated using EPA standard pitchblend ore in the same geometry as the samples. Excess ^{210}Pb was calculated by subtracting the activity of ^{214}Pb (352 KeV), a measure of supported ^{210}Pb, from the total ^{210}Pb (46.3 KeV) activity. All values of excess ^{210}Pb were decay corrected (22.3-year half life) to the date of core collection. A correction for self-adsorption of the low-energy ^{210}Pb gamma rays was made using the method of Cutshall et al. (1983).

$^{239+240}$Pu was determined by alpha counting following the wet chemical and plating procedures of Livingston and Bowen (1979). Selected samples were analyzed for ^{239}Pu and ^{240}Pu isotopes using ICP-MS following the procedures described by Kenna (2002).

Results and Discussion

Activities of ^{210}Pb and $^{239+240}$Pu reach their maxima at or near the tops of the cores and decrease with increasing depth (Figure 2). In roughly half of the cores the maximum for each nuclide is present at a depth of roughly 3-4 cm, instead of at the surface. Maximum excess ^{210}Pb activities range from ~4 to ~8 dpm g^{-1}, while maximum $^{239+240}$Pu activities range from ~40 to ~140 dpm kg^{-1}. The excess ^{210}Pb inventories range from 33 to 82 dpm cm^{-2} (Table 1), higher than the steady state figure expected from fallout of 32 dpm cm^{-2} (assuming 1.0 dpm cm^{-2} yr^{-1}; Turekian et al., 1977). The $^{239+240}$Pu inventories range from 0.5 to 1.6 dpm cm^{-2} (Table 1), also higher than the value of 0.48 dpm cm^{-2} expected from direct fallout (Buesseler et al., 1985). The fact that the measured inventories of ^{210}Pb and $^{239+240}$Pu are higher than expected from direct atmospheric fallout in all cores other than core 8 implies recent sediment deposition and recent focusing at all of these sites. The atom ratio of ^{240}Pu/^{239}Pu measured on selected samples was 0.183+.005 (ignoring one outlier), indistinguishable from the value of 0.18 expected for stratospheric fallout (Buesseler et al., 1985). Activities of ^{234}Th are well in excess of the supported levels in the top 2 cm of each of these cores (data not shown). However, presence of subsurface maxima could not be assessed because the samples from below 2 cm depth were not counted until roughly one year after collection, well after any excess ^{234}Th would have been lost to decay (half life = 24 d). Porosities decrease with depth in the cores; most values are between 60% and 80% (range 39% to 87%).

In the discussion below these data are interpreted as driven primarily by bioturbation, using a numerical sediment-mixing model. First, evidence for extensive bioturbation is presented, and the case is made that the radionuclides are transported downward in the sediments to a much larger degree by bioturbation than by sedimentation. Next, some of the profiles are interpreted assuming only biodiffusive mixing is occurring Finally, some of the profiles are interpreted using two different models that simulate non-diffusive mixing by organisms that feed at the sediment surface and defecate below the sediment surface.

Some simple analyses of the radionuclide profiles suggest that they are significantly influenced by bioturbation. For example, if the ^{210}Pb profiles without subsurface peaks were assumed to be driven by sedimentation with no bioturbation they would yield sedimentation rate estimates of 0.7, 0.9 and 0.1 cm yr^{-1} for cores 4, 7 and 8, respectively. Sedimentation rates this high would result, however, in $^{239+240}$Pu peaks at depths of ~20, ~27 and ~3 cm (respectively) in these cores, which are not observed. Indeed, the maxima are at the sediment surface. The presence of the $^{239+240}$Pu maximum at the surface implies that the sedimentation rate is low. Deep penetration of both ^{210}Pb and $^{239+240}$Pu is most likely due, therefore, to bioturbation.

Additional evidence for bioturbation stems from the depths of penetration of excess ^{210}Pb and $^{230+240}$Pu. In sediments where ^{210}Pb and $^{239+240}$Pu can be used to provide chronological information, excess ^{210}Pb should be detected at a greater depth than $^{239+240}$Pu. This is because excess ^{210}Pb should be detectable in sediments 100 or more years old (4+ half

lives) while $^{239+240}$Pu should not be detectable in sediments older than 40-50 years old (these cores were collected ~40 years after the onset of fallout from atmospheric nuclear testing). As was discussed by Anderson et al. (1988), on plots of excess ^{210}Pb versus $^{239+240}$Pu, such data would fall on a trend with a positive intercept on the excess ^{210}Pb axis, because excess ^{210}Pb should be detectable in sediments too old to contain any detectable $^{239+240}$Pu. However, plots of excess ^{210}Pb versus $^{239+240}$Pu for these Massachusetts Bay sediments show no such intercept (Figure 3). There is some scatter, but typically the trends extend through the origin. The implication of these results, collectively, is that the nuclides have been redistributed within the sediments by some common process, most likely bioturbation, that leads to covariation of these nuclides. Indeed, x-radiographs of sediments from these sites commonly show evidence of tubes emplaced by burrowing organisms.

Numerical sediment mixing model

Radionuclide transport in sediments was described by a variation of the advection-diffusion equation, with sedimentation treated as a process of advection and bioturbation as a diffusive process. The equation follows:

$$\frac{\partial \rho A}{\partial t} = \frac{\partial}{\partial z}\left[\rho D_B \frac{\partial A}{\partial z}\right] - \frac{\partial s \rho A}{\partial z} - \rho \lambda A + \left[\frac{\partial \rho A}{\partial z}\right]_{nl} \qquad (1)$$

Where

ρ = sediment bulk density (g cm^{-3})

A = activity (dpm g^{-1})

t = time (yr)

z = depth (cm)

D_B = biodiffusive mixing rate ($cm^2\ yr^{-1}$)

s = sedimentation rate ($cm\ yr^{-1}$)

λ = decay constant (yr^{-1})

$[\frac{\partial \phi A}{\partial z}]_{nl}$ = unspecified "non-local" exchange process, where a process is called non-local when the material is transported a distance greater than the length scale over which the concentration of a tracer changes substantially (Boudreau, 1986). Specific processes will be indicated later in this paper, for various depths of the sediment, according to various models.

Equation 1 was solved numerically using a sediment mixing model whose origins can be traced to Santschi et al. (1980) but which was subsequently modified and most thoroughly described in Crusius (1992; (see also Crusius and Anderson, 1995)). The boundary conditions for this numerical treatment include:

$$\text{flux} = -\phi_0 D_{B0} [\frac{\partial A}{\partial z}]_0 + \phi_0 s_0 A_0 \qquad (2)$$

$$[\frac{\partial \phi A}{\partial z}]_{z3} = 0, \qquad (3)$$

where z3 is the deepest sediment depth modeled, as defined in Appendix 1. It is worth noting that this model assumes bioturbation mixes sedimentary solids and not bulk sediment, and that porosity is unaffected by bioturbation. This latter assumption has also been made in other recent work using sediment mixing models (Nie et al., 2001; Alperin et al., 2002), although it requires further evaluation (e.g. Mulsow et al., 1998).

This numerical treatment of bioturbation has several advantages over analytical solutions to equation 1. First, it offers a more realistic description of the sediments in that it allows varying porosity and bioturbation with depth. In addition, the numerical model allows a realistic, time-dependent input for $^{239+240}$Pu at each core site, patterned after the approach of Alperin et al. (2002). Briefly, Pu delivery to the seafloor was assumed to begin in 1950 and peak in 1963 (Figure 4), based on the fallout record and the observation that a component of the Pu fallout was rapidly transported to the seafloor (Livingston and Bowen, 1979; Santschi et al., 1980). Post-1963 delivery of Pu to the seafloor was inferred from the measured $^{239+240}$Pu inventory in the sediments, assuming that any Pu present in excess of the expected fallout was transferred to the seafloor through an intermediate reservoir with a ~15 year residence time (Robbins et al., 2000). The modeled Pu profiles are not very sensitive to the form of this input function because of the rapid bioturbation in this region. The ^{210}Pb flux, by contrast, was assumed constant over time, although the magnitude of the flux was varied from core to core to fit the measured inventories.

A brief description of the treatment of bioturbation is presented because this model is used in this work primarily to evaluate mixing processes. Biodiffusive mixing rates are parameterized as a function of an adjustable parameter in each of two depth intervals of near-surface sediment. In this manner, regions of rapid mixing (typically near the sediment surface), slow mixing and no mixing can be treated by the model. It is worth pointing out as well that the biodiffusive mixing rate is also parameterized as a function of sediment bulk density. Hence, in this model the bioturbation rate decreases with depth

even if the mixing parameter is held constant, if the porosity decreases with depth (see Santschi et al., 1980). The treatment of non-diffusive mixing processes will be discussed later in this paper.

Cores with nuclide maxima at the surface

The mixing model was first used to interpret the radionuclide data from the three cores in which activities decrease monotonically from the surface (cores 4, 7 and 8; Figure 2), and therefore might be adequately described by strictly diffusive bioturbation (data from core 11 were not modeled because of the unusual subsurface minimum). The model was also used to examine whether the radionuclide profiles could be used to estimate the sedimentation rate. Because downward transport of radionuclides can be achieved both by sedimentation and by bioturbation, bioturbation rates were allowed to assume lower values at the higher sedimentation rates. In this manner, model fits were achieved such that when increased downward transport of the radionuclides due to a higher sedimentation rate was assumed, the downward transport due to bioturbation was reduced to compensate. The net downward transport was roughly the same in each case. This is a more thorough test of whether sedimentation rates could be inferred from the data than a simple sensitivity test to sedimentation at a constant mixing rate, because we have no way of knowing *a priori* whether sedimentation or bioturbation is responsible for the observed downward transport. Model runs simulating both ^{210}Pb and $^{239+240}$Pu were carried out assuming sedimentation rates of 0, 0.1 and 0.3 cm yr^{-1}(these are the values at the depths below which porosity is invariant). Reasonable, albeit slightly different, fits to the ^{210}Pb and $^{239+240}$Pu data were obtained for cores 4 and 7 when the sedimentation rate

was 0, 0.1 and 0.3 cm yr^{-1} (Figure 5), although the model runs began to deviate from the data when the sedimentation rate was 0.3 cm yr^{-1}. The largest sedimentation rate used in the model runs, 0.3 cm yr^{-1}, can be thought of as an upper limit. This upper limit is consistent with a ^{14}C-based estimate of ~0.1 cm yr^{-1} for Station 33, close to the site of collection of core 4 (Bothner, unpublished data; Figure 1). For core 8, only the model run with negligible sedimentation yields a reasonable fit; the upper limit on the sedimentation rate implied by the data at this site is thus lower than at the other two sites because of the much lower mixing rate observed (Figure 5). A low accumulation rate at this site is consistent with the measured inventories of ^{210}Pb and $^{239+240}Pu$, both of which are close to that expected from atmospheric fallout. These model fits for cores 4, 7 and 8 demonstrate that the sedimentation rate cannot be accurately estimated by ^{210}Pb and $^{239+240}Pu$ data in these cores.

An important conclusion from this modeling exercise is that in slowly accumulating sediments with extensive bioturbation, sedimentation rates cannot be constrained well based on ^{210}Pb and $^{239+240}Pu$ data. An earlier study in sediments below continental shelf and slope waters off Cape Cod came to a similar conclusion (Anderson et al., 1988). However, this conclusion differs from that of a recent study of sediments from the continental slope near Cape Hatteras (Alperin et al., 2002), which suggested that sedimentation rates there could be constrained within 25-40% by ^{210}Pb and $^{239+240}Pu$ data. The authors of that study did not apparently test the sensitivity of their model results to simultaneous increase in sedimentation rate and decrease in deep mixing rate. Such a test would determine if these adjustments compensated for one another, as they do in this

work, yielding sedimentation rate estimates that are less well constrained than sensitivity to sedimentation alone would suggest. However there are at least two important differences between the nuclide profiles in that study and this one. First, few of the nuclide profiles in Alperin et al. (2002) show subsurface peaks in ^{210}Pb, features that complicate the interpretation of the cores in this work (see discussion below). Second, the study of Alperin et al. (2002) involved a number of cores with well-defined subsurface $^{239+240}$Pu peaks where the ^{210}Pb profile shows no such peak (hence the $^{239+240}$Pu peak may indicate a fallout maximum). Both of these factors may well have allowed a firmer constraint on sedimentation rates in that work than in this study.

One simple means that can be used to identify conditions under which the sedimentation rate can be inferred from profiles of ^{210}Pb is to evaluate the relative importance of ^{210}Pb burial below the mixed layer versus decay within the mixed layer. ^{210}Pb can only be used to provide sedimentation rate and time estimates in locations where ^{210}Pb is buried below the mixed layer prior to decay. Expressed another way, the residence time of sediments in the "mixed layer" must be shorter than the effective dating timescale of the radionuclide. In Massachusetts Bay, where bioturbation extends to a depth of 30 cm (Figures 2, 3), the sedimentation rate would have to be on the order of 0.3 cm yr^{-1} or higher in order for ^{210}Pb to be a useful chronometer (residence time in mixed layer = 30 cm/0.3 cm yr^{-1} = 100 years = effective dating timescale of ^{210}Pb). Clearly, deeper mixed layers require higher sedimentation rates in order for ^{210}Pb to provide useful chronological information. This assessment of the relative importance of burial versus

decay is essentially equivalent to evaluation using the Second Damkohler number (Da (II)), where Da(II) = □L/s (Domenico, 1977), where L is the length scale of the mixing.

Cores with subsurface nuclide maxima

Radionuclide profiles from cores 5, 6, 9 and 14 contain well-defined subsurface maxima of ^{210}Pb and in most cases $^{239+240}$Pu. The subsurface maxima for $^{239+240}$Pu could conceivably reflect the maximum in fallout, but since they always coincide with maxima in ^{210}Pb (whose input is essentially constant), another process is almost certainly responsible. We can rule out a recent decrease in ^{210}Pb flux as a possible cause because such a decrease would have to have been sustained for decades, which is hard to envision and has never been reported in other settings. Another cause that we can virtually rule out is that these cores somehow reflect recent deposition of a large amount of nuclide-poor material (e.g., coarse sands). This mechanism would require deposition of extremely large amounts of nuclide-poor material over a large region of coastal waters reaching from Boston to Cape Cod, while leaving other areas of the region unaffected. This scenario seems extremely unlikely. Yet another possible process that could contribute to the subsurface peaks is diagenetic mobility of ^{210}Pb from surface sediments and re-immobilization at a depth of three or four cm. While mobility of ^{210}Pb cannot be discounted, we suggest this scenario is unlikely because it would require ^{210}Pb immobilization at a consistent depth in the various cores, and it would require similar mobility of ^{210}Pb and $^{239+240}$Pu, each of which is thought to be strongly particle-reactive. Finally, we consider trawling to be an unlikely cause of the subsurface maxima. While subsurface maxima in ^{7}Be profiles have been attributed to trawling in the past, (Mayer et

al., 1991), it is hard to imagine that a machine as destructive and non-selective as a trawl could reorient the surficial sediment as carefully and systematically as would be required to achieve the smooth subsurface maxima observed in the ^{210}Pb profiles of cores 5, 6, 9 and 14 (Figure 2).

The most likely cause of the subsurface peaks is mixing induced during subsurface ejestion of material by organisms that feed at or near the sediment surface and defecate below the surface. This mechanism has been invoked by other researchers to explain similar observations in a variety of locations (e.g., Aller et al., 1976; Boudreau, 1986; Smith et al., 1986; Sayles et al., 2001). Further evidence that such mixing occurs in Massachusetts Bay sediments is provided by occasional shoulders in the ^{234}Th profiles at the same depth as the ^{210}Pb peak (Bothner, unpublished data).

There are two slightly different mechanisms that could achieve such sub-surface peaks, each with different implications for the activity profile of ^{234}Th. According to one mechanism, the subsurface maximum occurs when a significant portion of the radionuclide flux to the seafloor is instantly redirected away from the surface, as it is consumed by surficial deposit feeders, and released during defecation at a depth below the sediment surface (similar to model 4a in Soetaert et al., 1996 and to Sayles et al., 2001). According to the other scenario, surficial sediment of a defined depth range is diverted with a variable rate constant to a defined depth range below the surface (Smith et al., 1986; model 5 in Soetaert et al., 1996). In either case, a subsurface maximum of ^{210}Pb and $^{239+240}$Pu occurs if enough of the high-activity, recent material is diverted away

from the surface of the sediment. In each case we assume that the sedimentation rate remains unaltered by this subsurface injection, as would be the case if the nuclides were associated with a small fraction of the total sediment, such as organic matter. Indeed, a mechanism similar to these two was previously identified as important in Massachusetts Bay in a study of artificially labeled sediments (Wheatcroft et al., 1994). The organisms thus far identified in nearby sediments that carry out this sort of mixing are cirratulid polychaetes, including *Tharyx acutus* (Myers, 1977) and *Cirriformia grandis* (Shull and Yasuda, 2001).

In order to demonstrate quantitatively whether the subsurface peaks in ^{210}Pb and $^{239+240}$Pu in these four cores (5, 6, 9, 14) could be driven by subsurface ejestion, the profiles were modeled by incorporating non-local mixing processes into the model. This mixing was first treated using the mathematics laid out in Robbins (1986) as described in Sayles et al. (2001), where the non-local mixing component is given by:

$$\left(\frac{\partial A}{\partial t}\right)_{nl} = G\exp\left\{\frac{-(z - z^*)^2}{2\sigma^2}\right\} \qquad (4)$$

z^* = depth of maximum nuclide insertion (cm)

σ = vertical extent of the nuclide input injected below the sediment surface (cm)

$G = \frac{f_n R}{\sqrt{2\pi\sigma^2}}$ = the rate of non-local input at the maximum,

where f_n is the fraction of nuclide flux diverted and R is the vertical rain rate of the nuclide.

Using this equation, the deposit feeders are assumed to defecate at depths that form a gaussian distribution with variance σ^2. Additional boundary conditions for this model include continuity of flux and of activity between layers.

A sensitivity test can be used to constrain the fraction of the nuclide flux diverted from the surface to subsurface depths. The sharp subsurface peaks in ^{210}Pb and $^{239+240}$Pu in many cores requires that the vast majority of the surface flux be diverted to the subsurface at these locations (fraction between 0.9 and 0.99; Figure 6 a, b). If the fraction diverted is lower than this figure, the surface activities of ^{210}Pb and $^{239+240}$Pu are more similar to those at the defecation depth than observed. A consequence of such extensive diversion of the surface nuclide flux is that the vast majority of the excess ^{234}Th is also diverted, resulting in a prominent sub-surface peak (Figure 6c). The presence of some excess ^{234}Th below the surficial sediments cannot be ruled out, as it was not measured (see methods section). However, the presence of large amounts of excess ^{234}Th in the top two centimeters of the cores is inconsistent with such a pronounced diversion of the nuclide flux. Instead, the observed high activities of ^{234}Th in surficial sediments can most readily be explained if recent material is deposited on the seafloor and is transported over a period of time to subsurface depths. A revision of the model discussed above attempts to simulate this process.

In this model the non-local mixing term assumes removal of radionuclide in a region near the sediment surface by a first order process according to:

$$\left[\frac{\partial A}{\partial t}\right]_{nl} = -irc \bullet \beta \bullet A \qquad (5)$$

where

irc = ingestion rate constant (sec^{-1}) in the surficial sediments (defined as the depth range from 0 cm to any depth).

This ingested material is then immediately transferred to subsurface sediments over a prescribed depth range, according to:

$$\left[\frac{\partial A}{\partial t}\right]_{nl} = \frac{\int_0^{uptakez} irc \bullet \phi \bullet A_0 \bullet dz}{insertzbottom - insertztop} \qquad (6)$$

Additional boundary conditions for this model include continuity of flux and of activity between layers. This treatment of subsurface ejestion is essentially identical to that presented by Smith et al. (1986) and in model 5 of Soetaert et al. (1996).

A sensitivity test demonstrates the primary controls on the shapes of the nuclide profiles. Results of this model are relatively sensitive to the ingestion rate constant. The pronounced subsurface maximum of both ^{210}Pb and $^{239+240}$Pu requires an ingestion rate constant on the order of 0.5 yr^{-1} or higher (Figure 7 j,k). Yet, despite the subsurface maximum in ^{210}Pb and $^{239+240}$Pu, the ^{234}Th maximum remains at the sediment surface, as is presumed to occur in these cores. The surface maximum in ^{234}Th activity persists because the modeled ingestion rate constants of 0-5-0.9 yr^{-1} lead to slow transfer of surficial sediment relative to the ^{234}Th half-life of 24 d. The model can also be used to evaluate processes causing downward transport of ^{210}Pb and $^{239+240}$Pu, including biodiffusive mixing and a broad defecation range (Figure 7 a,b,d,e). Either biodiffusive mixing on the order of 0.4 cm^2 yr^{-1} or more, or defecation spanning a depth range of several cm, lead to a pronounced subsurface maximum above five cm as well as

considerable nuclide transport below 10 cm. It is difficult to distinguish between these two processes with the model, since the effects are similar. However, both processes are probably occurring; in order to deposit material at depth, some sort of burrow must be constructed. Deep mixing must be occurring during burrow construction, and perhaps by other organisms, as well. The model results are relatively insensitive to the vertical extent of the "surficial" sediments; profiles differ only slightly when "surficial" is defined to extend from the surface to 0.5, 1 or 2 cm (Figure 7 g-i). It is worth noting that a minor subsurface ^{234}Th peak occurs on the shoulder of the surface maximum when the ingestion rate constant is 12 yr^{-1} (ingestion timescale of one month; Figure 7 l). Although excess ^{234}Th was not measured below a depth of 2 cm in these cores (see methods section), profiles from other cores from Massachusetts Bay show a subsurface peak similar to that presented in Figure 7l (Bothner, unpublished data), suggesting surficial material can be transported to subsurface depths in as little as one month.

Because this non-local model reproduced the general features of the ^{210}Pb, $^{239+240}$Pu and ^{234}Th profiles, this model was chosen as the best means to simulate the profiles with subsurface peaks (cores 5, 6, 9 and 14). The goal of the modeling was to determine whether reasonable choices of model parameters could reproduce the general features of the profiles, as an aid in identifying important processes occurring in the sediment. The same model parameters were used to simulate the ^{210}Pb and $^{239+240}$Pu profiles for each of the cores. The general features and the approximate shape of the ^{210}Pb and $^{239+240}$Pu profiles were achieved (Figure 8) by assuming nuclide uptake occurs from 0-1 cm, defecation from 2.5 to 3.5 cm, an ingestion rate constant of 0.3-0.9 yr^{-1} and moderately

high biodiffusive mixing (Figure 8) (see Appendix 2 for the complete set of parameter values). It is worth pointing out, as did Smith et al. (1986) that subsurface $^{239+240}$Pu peaks predicted by this model are more pronounced than are predicted subsurface ^{210}Pb peaks, when using the same input parameters. By contrast, the measured activities in some cores (especially core 5) reveal more pronounced subsurface peaks in ^{210}Pb activity than in $^{239+240}$Pu activity. In these cases, no choice of model parameters can yield a good fit of both the ^{210}Pb and $^{239+240}$Pu profiles. The cause of the sharper-than-predicted ^{210}Pb peaks is not clear, but could be due to either oversimplifications of the model or diagenetic mobility of ^{210}Pb.

This subsurface egestion model is thus reasonably consistent with all available constraints provided by the shapes of the profiles of ^{210}Pb, $^{239+240}$Pu and ^{234}Th in cores 5, 6, 9 and 14 (Figure 8). Furthermore, the set of processes described by the model is entirely consistent with previous discussions of important bioturbation processes in this setting (Wheatcroft et al., 1994). It is worth pointing out, however, that these model solutions are not unique. A variety of combinations of defecation range and biodiffusive mixing rate would yield very similar simulations. Overcoming this uncertainty will require a better understanding of the organisms and mechanisms causing mixing.

The model fits for all cores are summarized in Figure 8 while the values of the parameters are summarized in Appendix 2. In all cores other than core 8, the mass accumulation rates were chosen to achieve sedimentation rates of 0.1 cm yr^{-1} below the depth at which porosity remains constant. In core 8 a sedimentation rate of 0 cm yr^{-1} was

assumed, as discussed earlier. The good fit for all cores suggests that it is reasonable to assume biodiffusive mixing in roughly half of the cores (cores 4, 7 and 8), and mixing by surface injestion and subsurface ejestion, together with biodiffusive mixing, in the other half of the cores (cores 5, 6, 9 and 14).

Implications of mixing by subsurface egestion

There are many important implications of the bioturbation inferred in Massachusetts Bay sediments. First, the well-defined nature of the subsurface ^{210}Pb maximum implies that the material buried persists for many years. This is inconsistent with the notion that subsurface ejestion occurs due to temporary (seasonal) food caching by benthic organisms, as has been suggested by previous studies (Wheatcroft et al., 1994), unless only a small portion of the buried material is eventually used as food. There are also a number of implications for redox conditions implied by this deep mixing. Rapid mixing of material to depths of >15 cm in a few months, as observed by Wheatcroft et al. (1994) and modeled here, could provide a mechanism to divert labile organic matter from the oxic environment of the sediment surface to the typically reducing environment occurring at depths of tens of centimeters (Jumars et al., 1990). This labile organic matter could fuel diagenetic processes driven by the electron acceptors that are important at these depths, such as sulfate and manganese and iron oxyhydroxides. Furthermore, rapid transport of metals to significant depths may impact their diagenetic mobility. Mobility of Ag, Cu and Pb has been suggested to occur in these sediments (L. Kalnejais, personal communication, 2003), complicating the interpretation of the sedimentary concentrations of these metals and possibly leading to a flux into the bottom water.

There are also implications for the solid-phase record of contaminants. Mixing by any process to the observed depth of tens of centimeters severely reduces the temporal resolution obtainable from sedimentary records. In these sediments, only a crude estimate of the 100-year depth is possible. In addition, mixing by subsurface ejestion causes a portion of the recent contaminant flux to the seafloor to be diverted from the sea floor to depths of many centimeters. Instead of being vulnerable to resuspension during storms, this diverted portion would be buried below the depth reached by resuspension. Finally, non-local transport of contaminated sediment implies that surficial sediments will not accurately record changes in contaminant deposition.

In summary, the sediments of Massachusetts Bay are mixed by benthic organisms to a degree that sedimentation rates (and therefore sediment ages), cannot be reliably obtained from profiles of ^{210}Pb and $^{239+240}$Pu. In some cores a simple model invoking biodiffusive mixing to a depth of 30-35 cm can interpret the profiles. In a number of cores, however, coincident subsurface maxima in ^{210}Pb and $^{239+240}$Pu cannot be described by a biodiffusive mixing process but are consistent with insertion of recent material below the sediment surface by defecating organisms, as has been inferred by previous work. This type of deep mixing must have profound effects on redox conditions in the sediments, on the lability of organic matter within this "mixing zone" in the sediments, and on the distribution of recently deposited contaminants.

Acknowledgements

We wish to thank Adam Brown, Marilyn Buchholtz ten Brink, Anne Canaday, Ken Keay,

Carol Parmenter, Rick Rendigs and William Winters, for assistance in the field and with ^{210}Pb determinations and Alan Fleer, Juli Palmieri, Steve Pike and other members of Cafe Thorium at the Woods Hole Oceanographic Institution for Pu measurements. Steve Colman and John Bratton provided constructive comments on the manuscript. This work was conducted under a joint funding agreement between the USGS and the Massachusetts Water Resources Authority. Any use of trade, product or firm names is for descriptive purposes only, and does not imply endorsement by the U.S. Government.

References

Aller, R.C. and Cochran, J.K., 1976. ^{234}Th/^{238}U disequilibrium in near-shore sediment: particle reworking and diagenetic time scales. Earth and Planetary Science Letters, 29: 37-50.

Alperin, M.J., Suayah, I.B., Benninger, L.K. and Martens, C.S., 2002. Modern organic carbon burial fluxes, recent sedimentation rates, and particle mixing rates from the upper continental slope near Cape Hatteras, North Carolina (USA). Deep-Sea Research Part II-Topical Studies in Oceanography, 49(20): 4645-4665.

Anderson, R.F., Bopp, R.F., Buesseler, K.O. and Biscaye, P.E., 1988. Mixing of particles and organic constituents in sediments from the continental shelf and slope off Cape Cod: SEEP-I results. Cont. Shelf Res., 8: 925-946.

Bothner, M.H., Gill, P.W., Boothman, W.S., Taylor, B.B. and Karl, H.A., 1997. Chemical and textural characteristics of sediments at an EPA reference site for dredged material on the continental slope SW of the Farallon Islands. Open File Report 97-87, U.S. Geological Survey.

Bothner, M., Buchholtz ten Brink, M. and Manheim, F.T., 1998. Metal concentrations in surface sediments of Boston Harbor- Changes with time. Mar. Environ. Res., 45: 127-155.

Boudreau, B.P., 1986. Mathematics of tracer mixing in sediments: I. Spatially-dependent, diffusive mixing. American Journal of Science, 286: 161-198.

Boudreau, B.P., 1986. Mathematics of tracer mixing in sediments: II. Nonlocal mixing and biological conveyor-belt phenomena. American Journal of Science, 268: 199-238.

Buesseler, K.O., Livingston, H.D. and Sholkovitz, E.R., 1985. ^{239,240}Pu and excess ^{210}Pb inventories along the shelf and slope of the northeast U.S.A. Earth and Planetary Science Letters, 76: 10-22.

Crusius, J., 1992. Evaluating the mobility of ^{137}Cs, $^{239+240}$Pu and ^{210}Pb from their distributions in laminated sediments. Ph.D. Thesis, Columbia University, New York, 253 pp.

Crusius, J. and Anderson, R.F., 1995. Evaluating the mobility of ^{137}Cs, $^{239+240}$Pu and ^{210}Pb from their distributions in laminated lake sediments. Paleolimn., 13: 119-141.

Cutshall, N.H., Larsen, I.L. and Olsen, C.R., 1983. Direct analysis of ^{210}Pb in sediment samples: Self-adsorption corrections. Nucl. Inst. Methods, 26: 309-312.

Domenico, P.A., 1977. Transport Phenomena in Chemical Rate Processes in Sediments. Annual Review of Earth and Planetary Sciences, 5: 287-317.

Jumars, P.A., Mayer, L.M., Deming, J.W., Baross, J.A. and Wheatcroft, R.A., 1990. Deep-sea deposit-feeding strategies suggested by environmental and feeding constraints. Philos. Trans. R. Soc. London, A., 331: 85-101.

Kenna, T.C., 2002. Determination of plutonium isotopes and neptunium-237 in environmental samples by inductively coupled plasma mass spectrometry with total sample dissolution. Journal of Analytical Atomic Spectrometry, 17: 1471-1479.

Livingston, H.D. and Bowen, V.T., 1979. Pu and Cs-137 in coastal sediments. Earth Planet. Sci. Lett., 43: 29-45.

Mayer, L.M., Schick, D.F., Findlay, R.H. and Rice, D.L., 1991. Effects of commercial dragging on sedimentary organic matter. Marine environmental research, 31(4): 249-261.

Mulsow, S., Boudreau, B.P. and Smith, J.N., 1998. Bioturbation and porosity gradients. Limnol. and Oceanogr., 43(1): 1-9.

Myers, A.C., 1977. Sediment processing in a marine subtidal sandy botom community: I. Physical aspects. Journal of Marine Research, 35(3): 609-635.

Nie, Y.H., Suayah, I.B., Benninger, L.K. and Alperin, M.J., 2001. Modeling detailed sedimentary Pb-210 and fallout Pu-239,Pu-240 profiles to allow episodic events: An application in Chesapeake Bay. Limnology and Oceanography, 46(6): 1425-1437.

Pamatmat, M.M., 1971. Oxygen consumption by the seabed, IV. Shipboard and laboratory experiments. Limnol. and Oceanogr., 16: 536-550.

Robbins, J.A., 1978. Geochemical and geophysical applications of radioactive lead. In:

J.O. Nriagu (Editor), The biogeochemistry of lead in the environment. Elsevier, pp. 285-393.

Robbins, J.A., 1986. A model for particle-selective transport of tracers in sediments with conveyor belt deposit feeders. J. Geophys. Res., 91: 8542-8558.

Robbins, J.A. et al., 2000. Time-averaged fluxes of lead and fallout radionuclides to sediments in Florida Bay. Journal of Geophysical Research-Oceans, 105(C12): 28805-28821.

Santschi, P., H., Li, Y.-H., Bell, J.J., Trier, R.M. and Kawtaluk, K., 1980. Pu in coastal marine environments. Earth and Planet. Sci. Lett., 51: 248-265.

Sayles, F.L., Martin, W.R., Chase, Z. and Anderson, R.F., 2001. Benthic remineralization and burial of biogenic SiO_2, $CaCO_3$, organic carbon, and detrital material in the Southern Ocean along a transect at 170 degrees West. Deep-Sea Research Part Ii-Topical Studies in Oceanography, 48(19-20): 4323-4383.

Shull, D.H. and Yasuda, M., 2001. Size-selective downward particle transport by cirratulid polychaetes. Journal of Marine Research, 59(3): 453-473.

Smith, J.N., Boudreau, B.P. and Noshkin, V., 1986. Plutonium and ^{210}Pb distributions in Northeast Atlantic sediments: Subsurface anomalies caused by non-local mixing. Earth and Planetary Science Letters, 81: 15-28.

Soetaert, K., Herman, P. M. J., Middelburg, J. J., Heip, C., deStigter, H. S., vanWeering, T. C. E., Epping, E., Helder, W., 1996. Modeling Pb-210-derived mixing activity in ocean margin sediments: Diffusive versus nonlocal mixing. J. Mar. Res., 54(6): 1207-1227.

Wheatcroft, R.A., Olmez, I. and Pink, F.X., 1994. Particle bioturbation in Massachusetts Bay - preliminary results using a new deliberate tracer technique. Journal of Marine Research, 52(6): 1129-1150.

Turekian, K.K., Nozaki, Y. and Benninger, L.K., 1977. Geochemistry of atmospheric radon and radon products. Ann. Rev. Earth Planet. Sci., 5: 227-255.

Appendix 1: A brief description of each parameter is given below. For a more thorough description see Crusius, 1992 or Santschi et al., 1980. The last eight parameters are included in this model for the first time, but are equivalent to those used in the models of Soetaert et al. (1996) and Sayles et al. (2001).

z1	bottom depth of top mixed layer (cm)
z2	bottom depth of secondary mixed layer (cm) (immediately below top mixed layer)
z3	bottom depth of modeled profile (cm)
r1	surficial sediment mixing parameter (g cm^{-2} yr^{-1}) that affects D_B
r2	mixing parameter (g cm^{-2} yr^{-1}) in secondary mixed layer; affects D_B
ar1	top mixing attenuation coefficient (cm^{-1})
ar2	deep mixing attenuation coefficient (cm^{-1}) in $D_B(z)$ = r2*exp(-ar2*depth)*mz/((1-p(z))*rs), for z1 < z < z2. The same form also holds for z < z1 (substituting r1 and ar1 for r2 and ar2)
pinf	porosity at infinite depth (cm^3 water/cm^3 total sediment)
p0	porosity increment
a	attenuation constant of porosity with depth, in overall porosity expression of p(z) = pinf+p0*exp(-a*z).
mz	model depth step (cm)
rs	sediment dry density (g cm^{-3})
MAR	mass accumulation rate (g cm^{-2} yr^{-1})
alr	decay constant (yr^{-1})
insertz	depth of maximum nuclide insertion by deposit feeders (cm)
sigma	breadth of distribution of deposit feeders (cm)
fraction	fraction of nuclide flux diverted to subsurface depth by deposit feeders
G	the rate of non-local input at the maximum (dpm cm^{-3} yr^{-1})
uptakez	depth of bottom of "surficial" sediment (cm)
irc	ingestion rate constant in surficial sediments (yr^{-1})
insertztop	the top of the defecation depth range (cm)
insertzbottom	the bottom of the defecation depth range (cm)

Appendix 2: Parameter values used in the numerical model runs presented in Figure 8. Cores 4, 7 and 8 assumed biodiffusive mixing only while cores 5, 6, 9 and 14 assumed surface injestion and subsurface defecation, together with biodiffusive mixing. Porosities were fit to measured porosities. The mass accumulation rates (MAR) were fixed at the value that gave a linear sedimentation rate of 0.1 cm yr^{-1} below the depth at which porosity stops changing, except for core 8, where negligible sedimentation was assumed. The decay constants (alr) include values for ^{210}Pb (0.0311) and $^{239+240}Pu$ (0.0001).

parameter	**4**	**5**	**6**	**7**	**8**	**9**	**14**
z1	10	2	4	2	2	5	4
z2	23	23	35	30	25	25	25
z3	45	40	45	40	40	40	40
r1	60	17	20	30	2	10	10
r2,	5	17	20	30	2	4	4
ar1	0	0	0	0	0	0	0
ar2	0	0	0	0	0	0	0
pinf	0.74	0.49	0.52	0.74	0.77	0.38	0.57
p0	0.14	0.34	0.31	0.12	0.13	0.26	0.26
a	0.15	0.1	0.1	0.1	0.5	0.1	0.1
mz	0.2	0.1	0.1	0.2	0.2	0.1	0.1
rs	2.5	2.5	2.5	2.5	2.5	2.5	2.5
MAR	0.065	0.13	0.12	0.065	10^{-6}	0.16	0.10
alr	0.0311, 10^{-4}	0.0311, 10^{-4}	0.0311, 10^{-4}	0.0311, 10^{-4}	0.0311, 10^{-4}	0.0311, 10^{-4}	0.0311, 10^{-4}
uptakez		1	1			1	1
irc	0	0.9	0.9	0	0	0.9	0.9
insertztop		2.5	2.5			2.5	2.5
insertzbottom		3.5	3.5			3.5	3.5

Table 1: Radionuclide inventories derived from the ^{210}Pb and $^{239+240}Pu$ profiles.

Core	Water depth (m)	excess ^{210}Pb inventory (dpm cm^{-2})	$^{239+240}Pu$ inventory (dpm cm^{-2})
fallout only		32[1]	0.48[2]
4	92	82	1.6
5	64	43	0.7
6	36	43	1.0
7	39	53	1.2
8	192	33	0.5
9	51	46	0.7
11	89	51	0.8
14	77	55	1.0

[1] steady-state ^{210}Pb inventory expected from a constant input of 1.0 dpm cm^{-2} yr^{-1}.
[2] from Buesseler et al., 1985.

Figure Legends

Figure 1: Map of Massachusetts Bay core locations. Large numbers indicate core locations, while small numbers indicate water depths (in m).

Figure 2: ^{210}Pb and alpha-counted $^{239+240}$Pu data from the Massachusetts Bay cores (solid squares). Open circles represent $^{239+240}$Pu data determined by ICP-MS. Error bars are 1-sigma uncertainties based on counting statistics. Two of six replicate Pu analyses carried out by both alpha spectrometry and icp-ms differ by more than the stated uncertainty. Note that the $^{239+240}$Pu horizontal scales vary.

Figure 3: Excess (xs) ^{210}Pb plotted versus $^{239+240}$Pu for each of the sediment cores. Note the absence of a clear intercept on the excess ^{210}Pb axis.

Figure 4: Annual $^{239+240}$Pu fallout used in the input functions for the $^{239+240}$Pu simulations in the numerical model, following the approach of Alperin et al. (2002). Fallout was assumed to commence in 1950 and continue until the date of core collection (1992).

Figure 5: Numerical model simulations for the data from Stations 4, 7 and 8, invoking depth-dependent biodiffusive mixing and sedimentation rates of 0 (open circles), 0.1 (solid circles) and 0.3 cm yr^{-1} (solid line with pluses). The same diffusion parameters were used for both the ^{210}Pb and the $^{239+240}$Pu simulations (see Appendix 2). Biodiffusive mixing rates are parameterized as a function of the bulk density, hence they decrease with depth wherever the porosity decreases with depth.

Figure 6: Sensitivity tests of the "diverted nuclide flux" model (Eq. 4) to variations in f_n (fraction of nuclide flux diverted from surface; a-c). Model parameters were as follows, except where indicated otherwise: depth of nuclide release = 3 cm; sigma = 0.5 cm; sed = 0 cm yr^{-1}; D_B = 0.1 cm^2 yr^{-1}; dry density = 2.5 g cm^{-3}; depth step = 0.1 cm; porosity of

core 14; squares represent an f_n of 0.9. This model is very similar to ones described in previous work (model 4a in Soetaert et al., 1996; Sayles et al., 2001).

Figure 7: Sensitivity tests of "surface ingestion and subsurface defecation" model (Eqs. 5-6) profiles to D_B (a-c), the range of defecation depths (d-e), the range of surface ingestion depths (g-i) and the ingestion rate constant (irc; j-l). Model parameters were as follows, except where indicated otherwise: ingestion range = 0-1 cm; defecation range = 2.5-3.5 cm; $D_B = 0.1$ cm^2 yr^{-1}; irc = 0.9 yr^{-1}; sed rate = 0 cm yr^{-1}; porosity of core 14. The unlabelled surface range is 0-1 cm (g-i), while the unlabelled irc is 0.5 yr^{-1} (j- l). Note a surface maximum of ^{234}Th in all model runs. The ^{234}Th simulations were numerically unstable under the conditions of large defecation range, hence they are not shown. This model is very similar to models described in previous work (Smith et al., 1986; model 5 in Soetaert et al., 1996).

Figure 8: Plots of mixing model simulations of the ^{210}Pb and $^{239+240}$Pu profiles for cores 4, 5, 6, 7, 8, 9 and 14, in addition to the biodiffusive mixing rates. Cores 4, 7 and 8 invoked only biodiffusive mixing, while cores 5, 6, 9 and 14 invoked surface injestion followed by subsurface defecation (Eqs. 5-6). Model parameters are presented in Appendix 2.

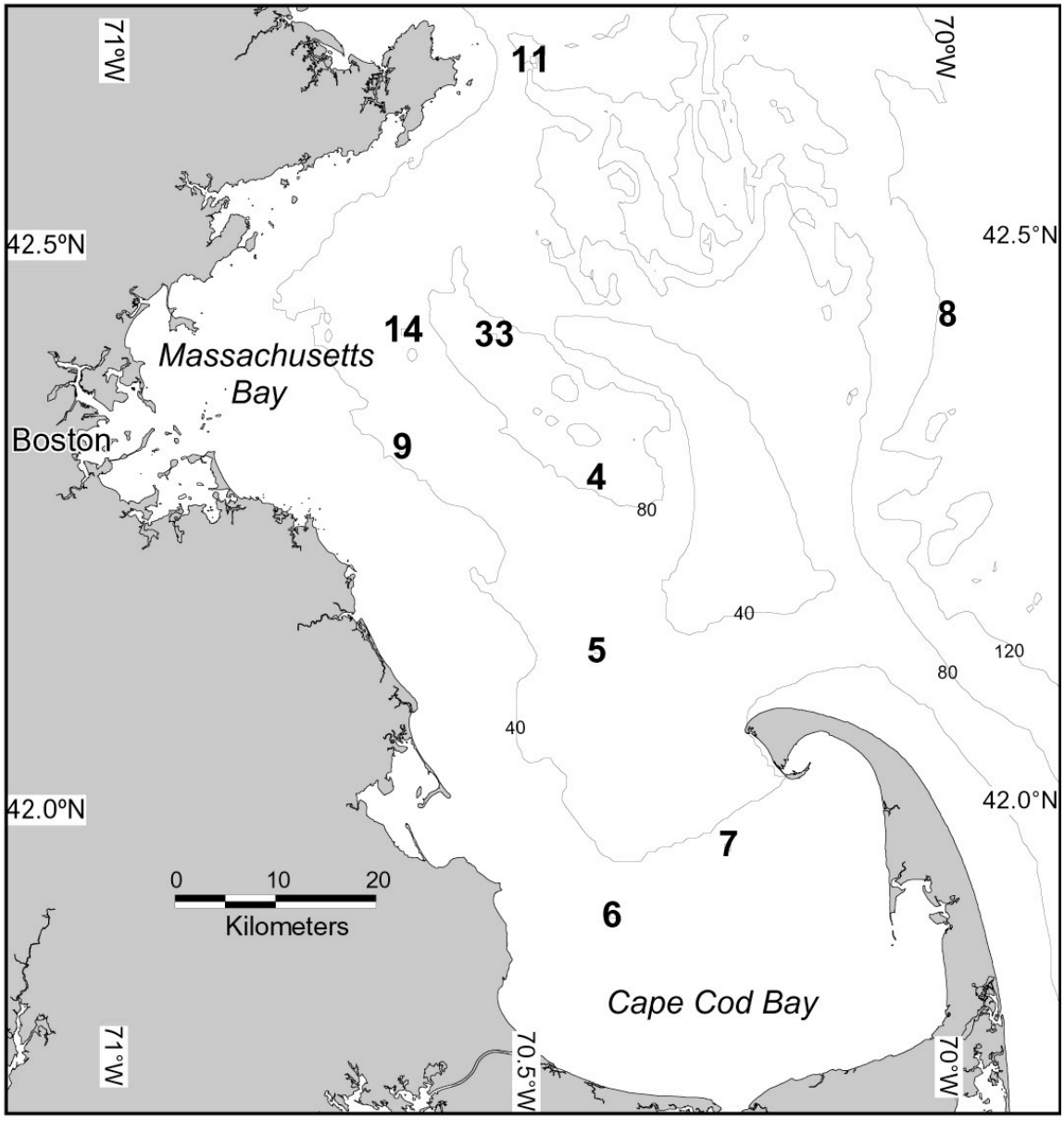

Crusius Fig 1

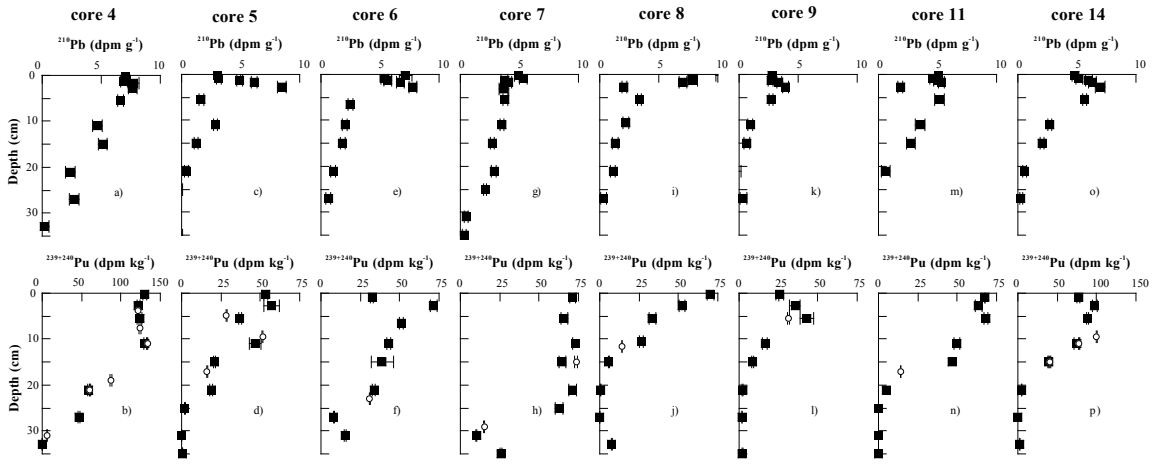

Crusius Fig 2 ^{210}Pb and $^{239+240}$Pu

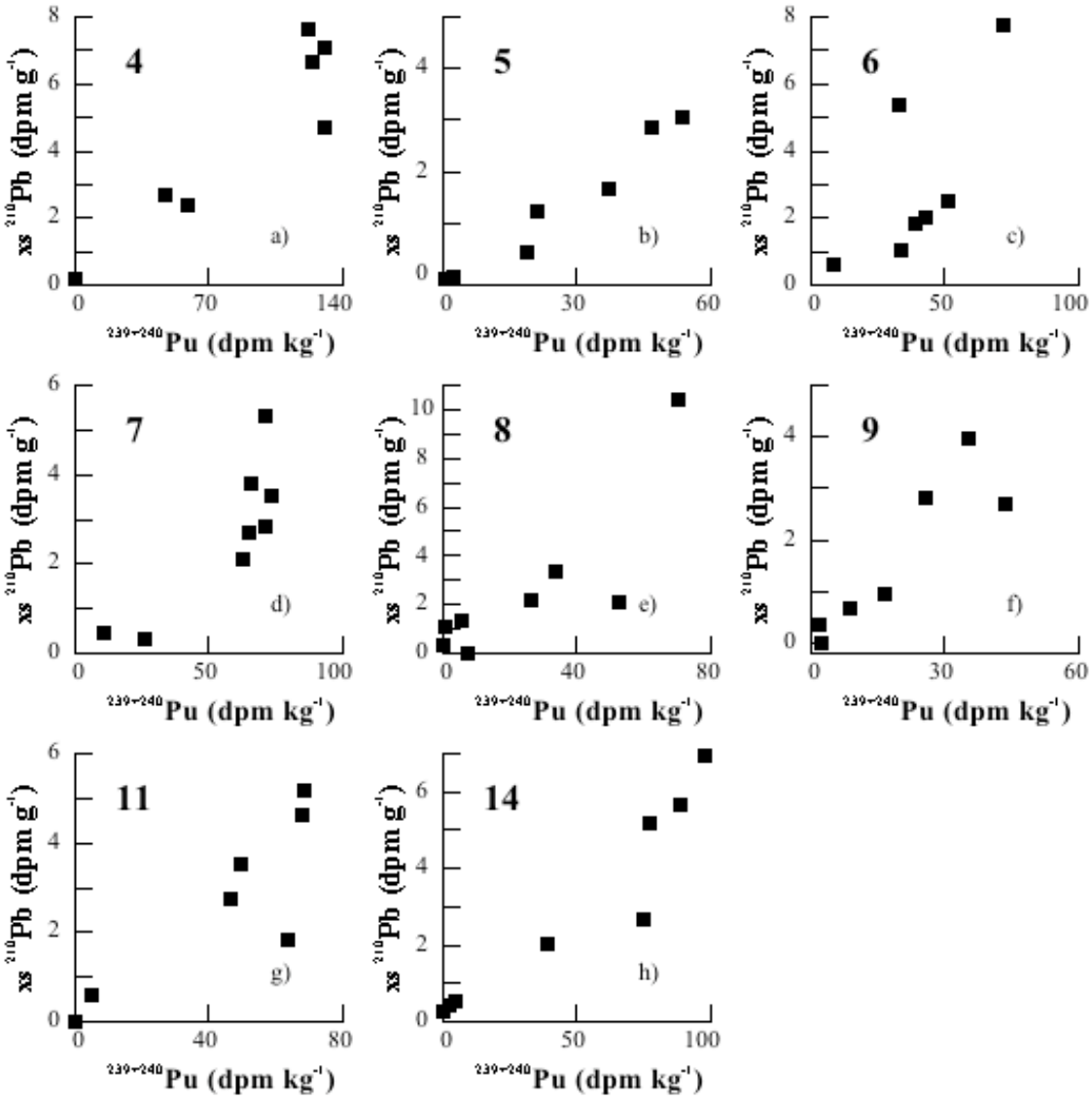

Crusius Fig 3 Pb vs Pu

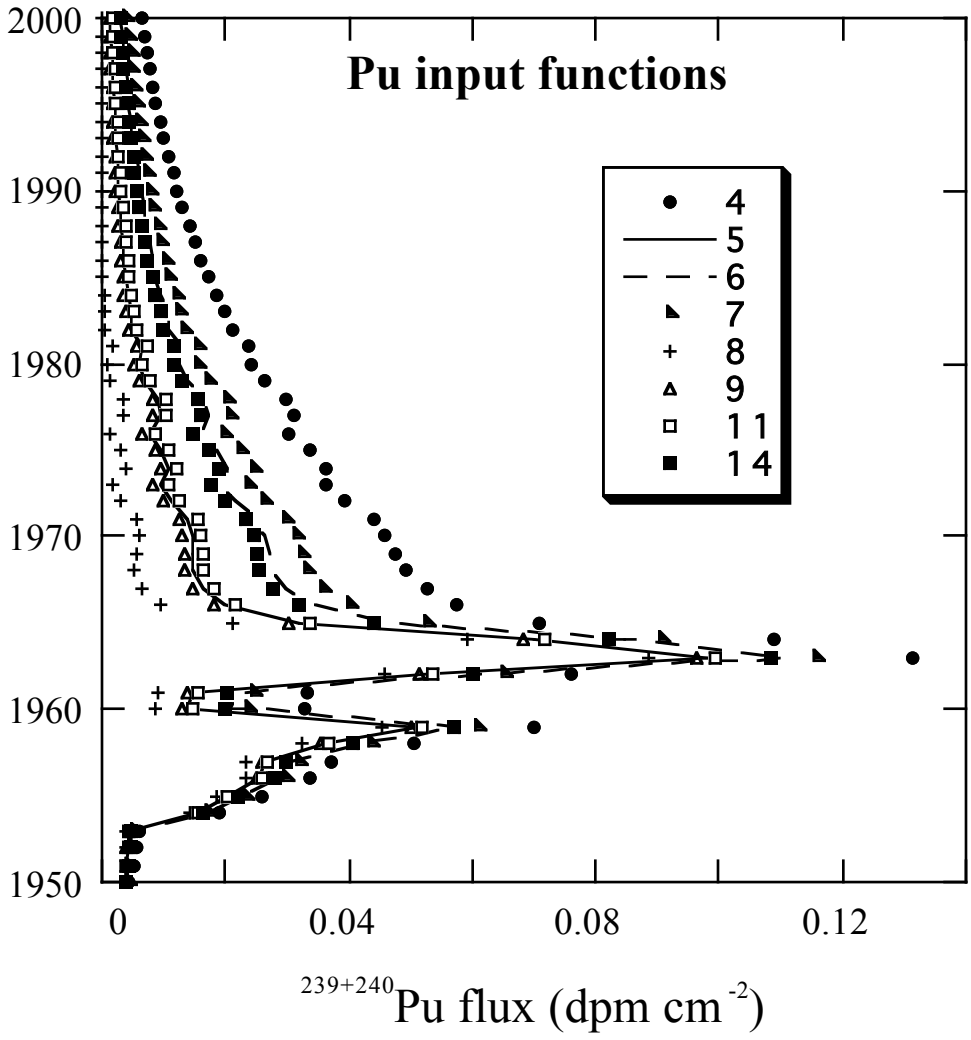

Crusius Fig 4 Pu input functions

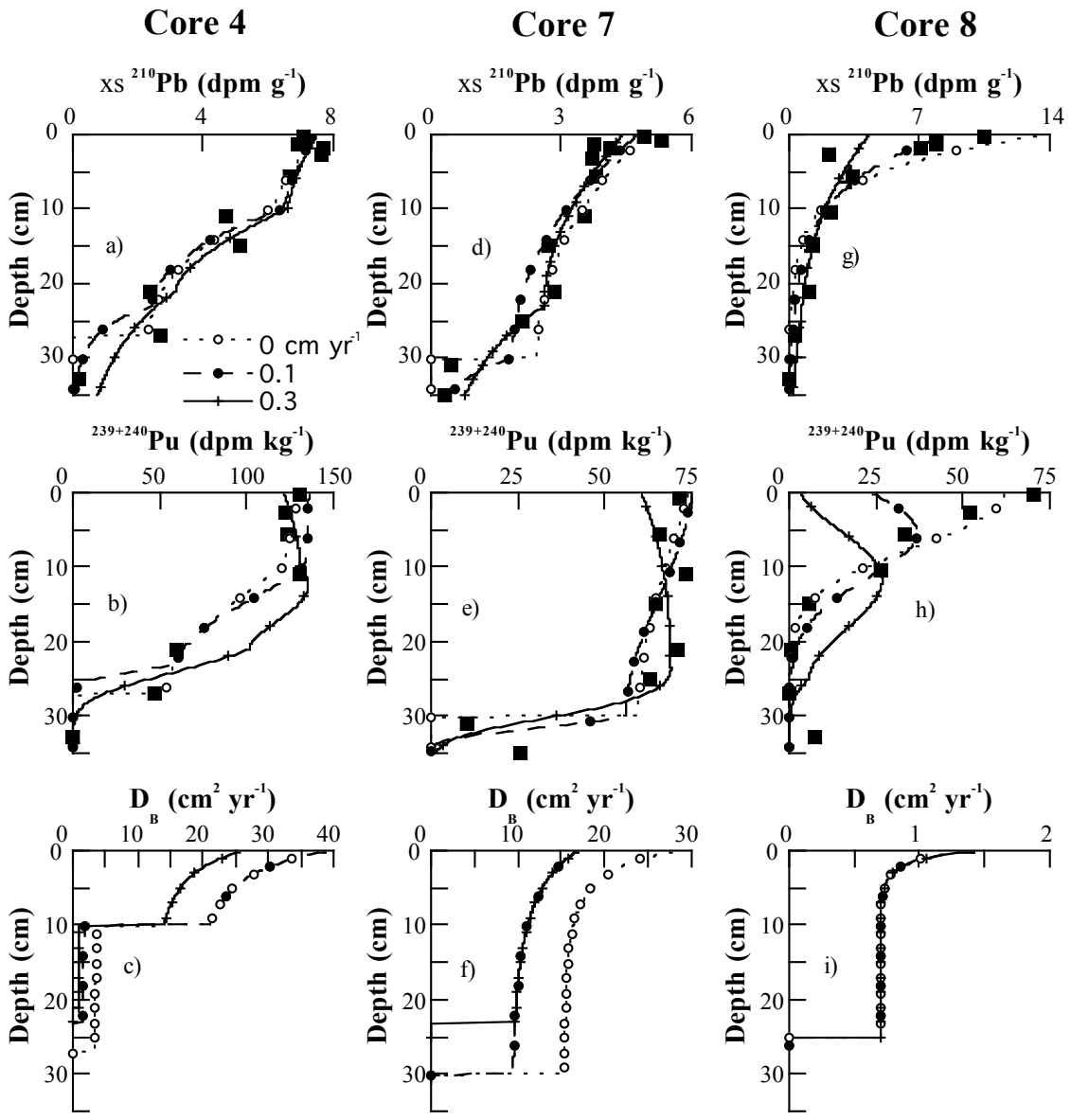

Crusius Fig 5 Cores 4, 7, 8 diffusive mix

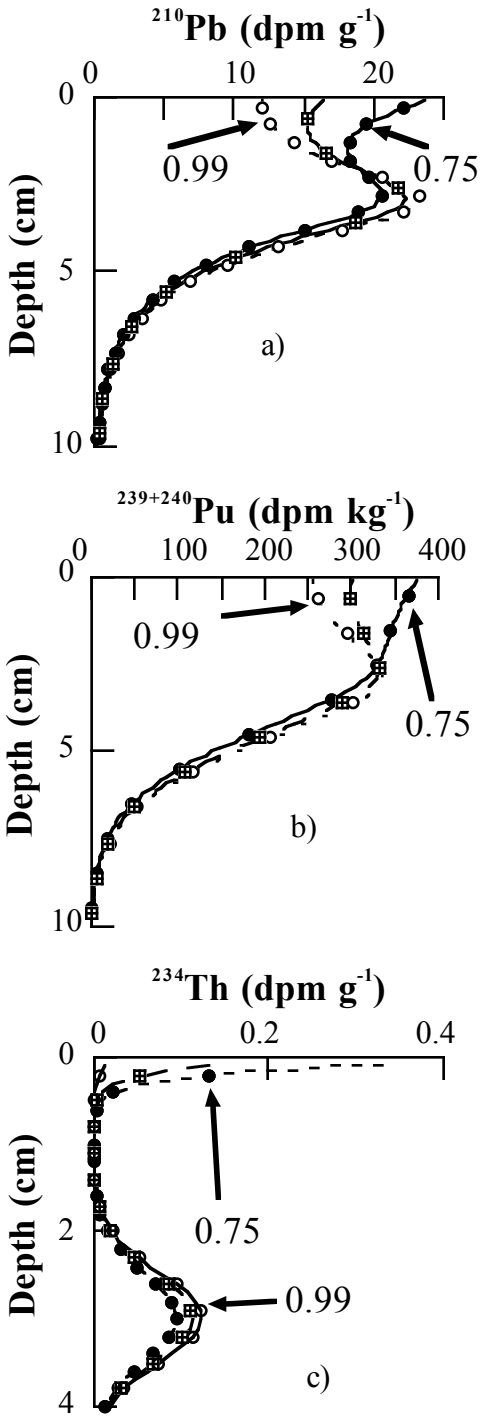

Crusius Fig 6 Sensitivity to fraction diverted

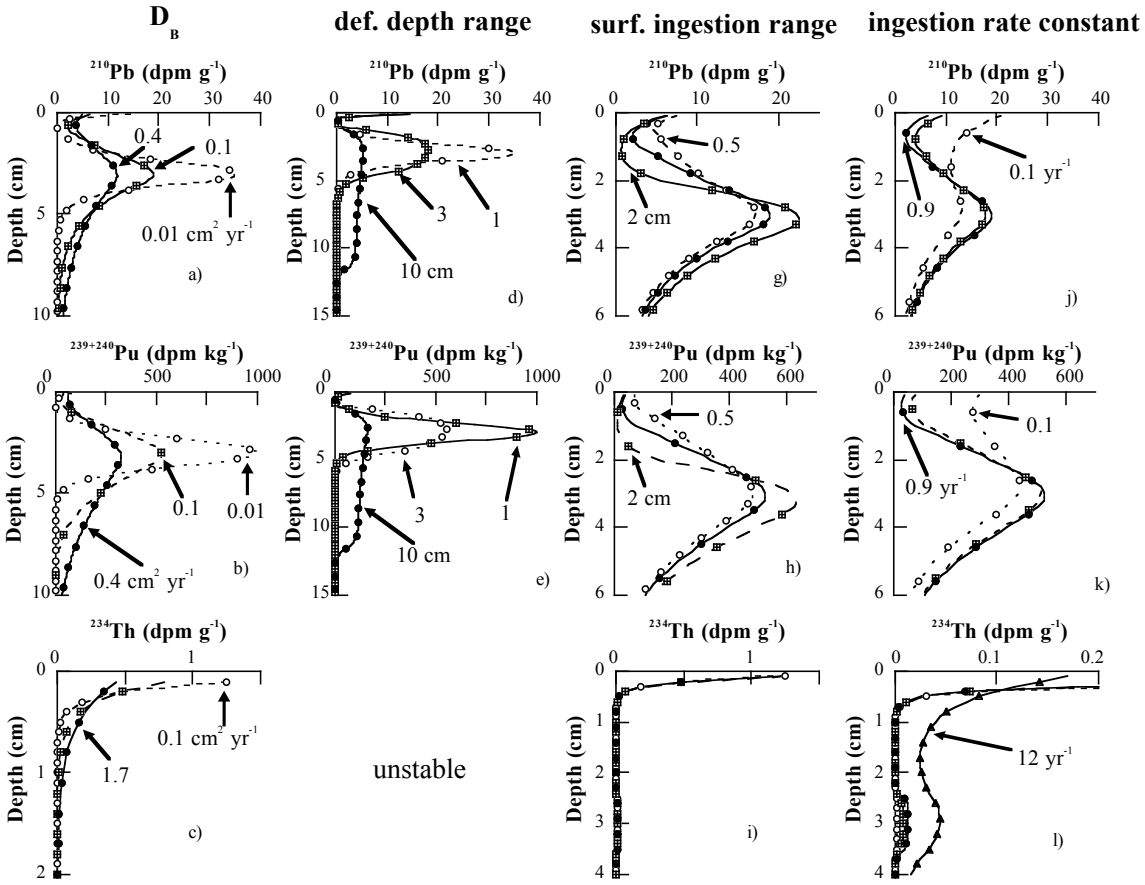

Figure 7 Crusius Sensitivity test, surface ingestion model

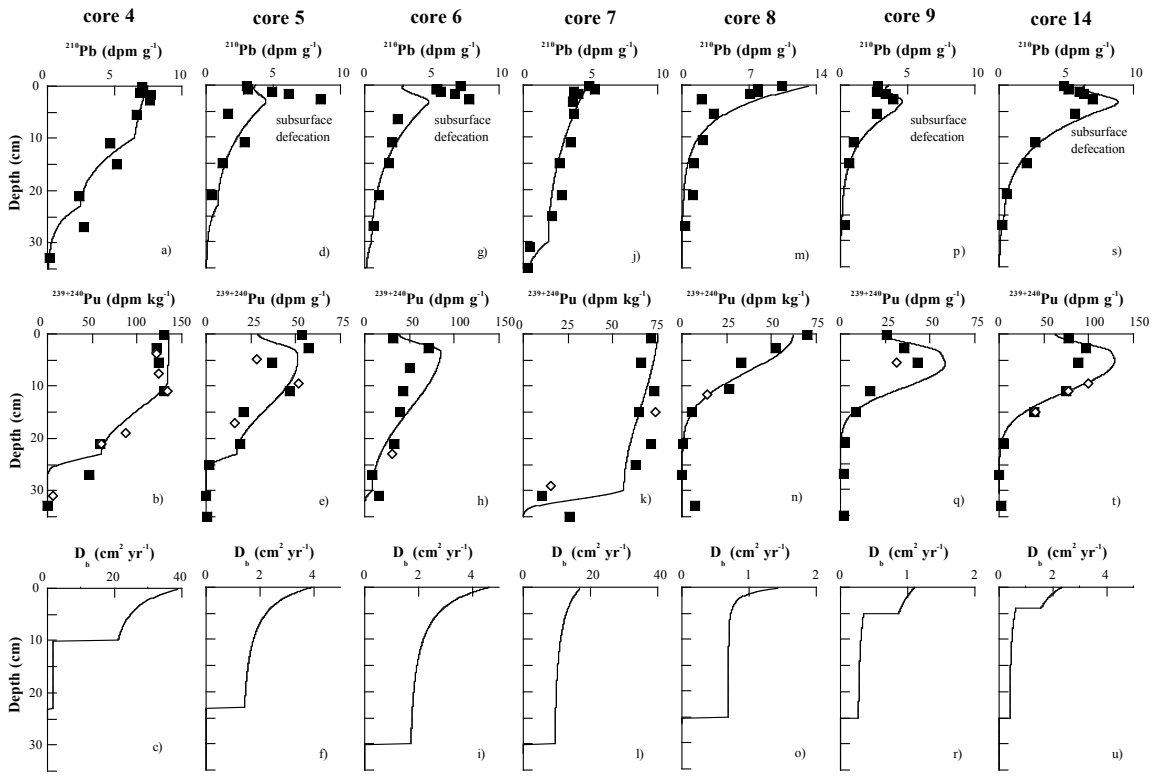

Figure 8 Crusius Best fits